Preprints (www.preprints.org) | NOT PEER-REVIEWED | Posted: 27 September 2019 doi:10.20944/preprints201909.0312.v1

Peer-reviewed version available at *Hydrology* **2020**, *7*, 9; doi:10.3390/hydrology7010009

Article

Simulating Flash Floods Using a Geostationary Satellite-Based Rainfall Estimation Coupled with a Land Surface Model

Dwi Prabowo Yuga Suseno [1]* and Tomohito J. Yamada [2]**

[1] Directorate Protected Forest Management Unit, Ministry of Environment and Forestry Republic of Indonesia, Gedung Manggala Wanabhakti Blok I Lantai 12, Jl. Gatot Subroto, Senayan, Jakarta 10270, Indonesia;

[2] Faculty of Engineering, Hokkaido University, N13 W8, Kita-ku, Sapporo, Hokkaido 060-0808, Japan

* Correspondence: dwiprab@gmail.com; Tel.: +62-021-570-4501; Fax: +62-021-573-3431

** tomohito@eng.hokudai.ac.jp; Tel.:+81-11-706-6188; Fax: +81-11-706-6188

Abstract: Clarifying hydrologic behavior, especially behavior related to extreme events such as flash floods, is vital for flood mitigation and management. However, discharge and rainfall measurement data are scarce, which is a major obstacle to flood mitigation. This study (i) simulated flash floods on a regional scale using three types of rainfall forcing implemented in a land surface model and (ii) evaluated and compared simulated flash floods with the observed discharge. The three types of rainfall forcing were those observed by the Automated Meteorological Data Acquisition System (AMeDAS) (Simulation I), the observed rainfall from the Ministry of Land, Infrastructure and Transportation (MLIT) (Simulation II), and the estimated rainfall from the Multi-purpose Transport Satellite (MTSAT), which was downscaled by AMeDAS rainfall (Simulation III). MLIT rainfall observations have a denser station network over the Ishikari River basin (spacing of approximately 10 km) compared with AMeDAS (spacing of approximately 20 km), so they are expected to capture the rainfall spatial distribution more accurately. A land surface model, Minimal Advance Treatments of Surface Interaction and Runoff (MATSIRO), was implemented for the flash flood simulation. The river flow simulations were run over the Ishikari river basin at a 1-km grid resolution and a 1-h temporal resolution during August 2010. The statistical performance of the river flow simulations demonstrated that Simulation I was reasonable compared with Simulation III. The findings also suggest that the advantage of the MTSAT-based estimated rainfall (i.e., good spatial distribution) can be coupled with the benefit of direct AMeDAS observations (i.e., representation of the true rainfall).

Keywords: MTSAT, LSM, heavy rainfall, flash flood

1. Introduction

Clarifying the hydrological behavior of a catchment area, especially behavior related to extreme events such as flash floods, is vital for flood mitigation and management. Some studies have focused on flash flood mitigation, including risk estimation [1], early detection [2], and severity [3,4]. The magnitude of peak discharge and time to peak discharge during flash flood events are important parameters that should be assessed to help mitigate their disastrous effect. This information is usually derived by analyzing discharge measurements. However, problems arise when the catchment is ungauged because the gauges are damaged by hazards. Rainfall-runoff models are used to simulate discharge as an alternative way to obtain hydrologic data.

Rainfall observation network data are commonly employed as input data for rainfall-runoff models. However, these data tend to be sparse and unevenly distributed in space. Other challenges to developing high-density and well-configured rain gauge networks include limited funds, site

© 2019 by the author(s). Distributed under a Creative Commons CC BY license.

Preprints (www.preprints.org) | NOT PEER-REVIEWED | Posted: 27 September 2019 doi:10.20944/preprints201909.0312.v1

Peer-reviewed version available at Hydrology 2020, 7, 9; doi:10.3390/hydrology7010009

accessibility, and network purposes [5]. Radar can be used to obtain the spatial distribution of rainfall, but this method is considered too expensive; high mountainous ranges can also block radar signals. Geostationary-based rainfall estimation is an alternative way to provide continuous rainfall information, particularly for ungauged catchments [6,7]. Geostationary satellite images blended with microwave satellite rainfall measurements are preferable to the sole use of microwave satellite-based rainfall measurements, because geostationary satellites provide the advantage of capturing global coverage with a continuous acquisition time, which is very useful for monitoring purposes. Geostationary-based rainfall estimation can be coupled with a rainfall-runoff model to predict the flood discharge produced by a catchment [8].

We conducted flash flood simulations based on a physical hydrological model called the Minimal Advance Treatments of Surface Interaction and Runoff (MATSIRO) [9]. MATSIRO uses physical processes to calculate the hydro-meteorological characteristics of a region, as expressed by energy balance and water balance models. It is a free and open source hydrological model which is possible for the user to make some modification. Several modifications of MATSIRO had been conducted such as incorporation of anthropogenic water regulation modules which is significantly improves river discharge simulation in the heavily regulated global river basins [10] and groundwater representation to simulate the major groundwater variables in the model [11]. The coverage of those studies is a global scale mainly in 1° × 1° spatial resolution. Here, the river flow estimation module in MATSIRO was applied for flash flood simulation on a regional scale, with a grid size is refined of approximately 1 km × 1 km.

In this study, we had two objectives. The first was to simulate flash floods on a regional scale using three types of rainfall forcing i.e., observation by sparse station, observation by dense station and satellite rainfall estimation which is downscaled by rainfall from sparse observation. Considering the density of rainfall network influence the accuracy significantly, our hypothesis is that the denser rainfall network will show the best performance. However, to arrange a dense and evenly distributed rainfall network could be costly and possibly not all the area can be covered due to accessibility reason. Here we combined the satellite rainfall estimation with the sparse rainfall data through downscaling procedure. We expect that the downscaled rainfall estimation will have a comparable performance with dense rainfall network, but operationally it will more cost effective than arranging a dense rainfall network. The second objective was to compare and evaluate the simulated river discharge with the observed discharge.

2. Brief Description of the MATSIRO and Forcing Data Preparation

MATSIRO simulates the energy balance that is determined separately at the ground surface and canopy surface, and the energy and water exchange between the ground surface and the atmosphere [9]. To simulate the energy balance as well as the water exchange, MATSIRO uses two components: LNDFLX for determining the parameters and calculating the surface fluxes, and LNDSTP for treating the ground processes. The schematic diagram of MATSIRO is shown in Figure 1 and it is explained as following.

Preprints (www.preprints.org) | NOT PEER-REVIEWED | Posted: 27 September 2019 doi:10.20944/preprints201909.0312.v1

Peer-reviewed version available at Hydrology 2020, 7, 9; doi:10.3390/hydrology7010009

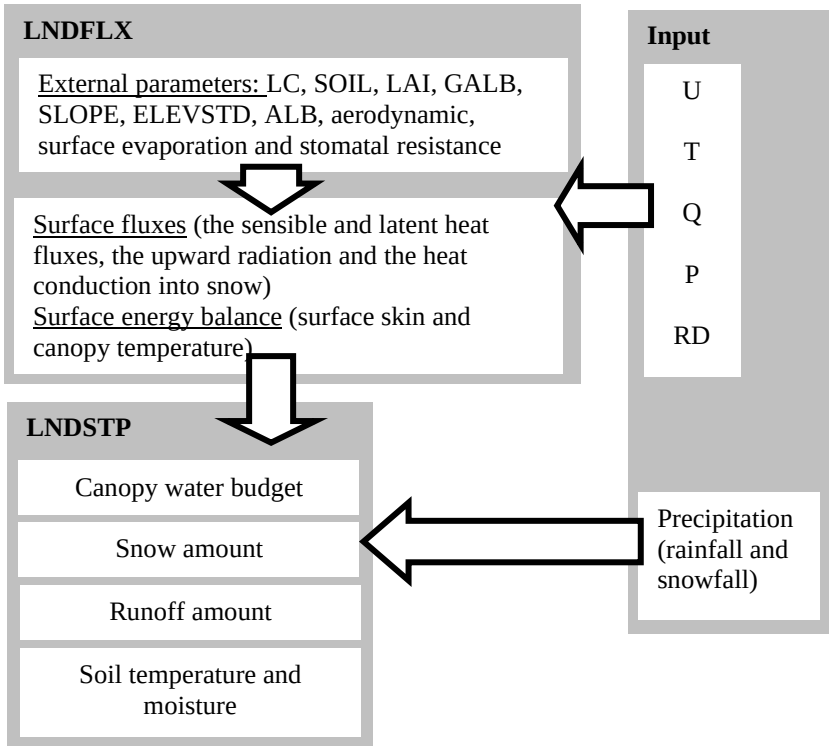

Figure 1. The structure and calculation flow in the MATSIRO (reproduced from Takata et al., 2003). The abbreviations is explained in the text.

LNDFLX assesses external parameters that are prescribed as horizontal distributions (maps), such as land cover type (LC), soil type (SOIL), leaf area index (LAI), ground albedo (GALB), surface mean slope (SLOPE), and standard deviation of altitude in a grid cell (ELEVSTD). Input variables such as precipitation, wind velocity (U), atmospheric temperature (T), humidity (Q), pressure (P), and downward radiation (RD) variable are set. Next, the albedo, the aerodynamic resistance, the surface evaporation resistance and the stomatal resistance are evaluated based on the radiative transfer in the canopy, turbulent transfer, and photosynthesis. These input variables are used to diagnose the surface fluxes (the sensible and latent heat fluxes, the upward radiation, and the heat conduction into snow) and the surface energy balance (surface skin and canopy temperature).

LNDSTP calculates the canopy water budget, snow amount, runoff amount, and soil temperature and moisture are calculated based on precipitation (rainfall and snowfall) using the fluxes obtained by LNDFLX as the upper boundary condition. Here, the runoff is generated by considering four different mechanisms: (i) the ground water runoff (base runoff); (ii) the saturation excess runoff (Dunne mechanism); (iii) the infiltration excess runoff (Horton mechanism); and (iv) the overflow of the surface soil layer. This runoff is then routed through the river network using the Total Runoff Integration Pathways (TRIP) method [12]. By this process, a river flow accumulation is generated at every time-step, and the estimated river flow (discharge) can be observed at any position in the region, particularly in the outlet of the catchment.

The original and modified MATSIRO which is previously explained mainly used global data that is derived from global atmospheric data set such as the NCC data forcing, Global Soil Wetness Project (GSWP-2), International Satellite Land Surface Climatology Project-Initiative II (ISLSCP-2), and International Geosphere-Biosphere Programme, and vegetation properties [11]. For a regional scale study those of data was considerably too coarse. Therefore, we focused on acquiring MATSIRO forcing data using remote sensing techniques. The application of remote sensing is also intended to overcome the problems associated with the shortage of observed data. Several types of remote sensing datasets were acquired for the MATSIRO forcing: the Moderate Resolution Imaging Spectroradiometer (MODIS), Shuttle Radar Topographic Mission Digital Elevation Model (SRTM-

Preprints (www.preprints.org) | NOT PEER-REVIEWED | Posted: 27 September 2019 doi:10.20944/preprints201909.0312.v1

Peer-reviewed version available at Hydrology 2020, 7, 9; doi:10.3390/hydrology7010009

DEM), Cloud and Earth's Radiant Energy System (CERES), and MTSAT images. Some primary and secondary data were also used, such as rainfall and meteorological observations, numerical weather prediction, and soil information.

Since we employed many different types of data with different spatial resolution and map projection, we performed pre-processing data by using aggregation, spatial resampling (dis-aggregation) and spatial interpolation techniques so as to they shared the same spatial resolution and projection. However, the impact of such pre-processing to the result was not discussed in this paper, because they were beyond to scope of this study. Table 1 briefly summarizes the data used in this study, including their source and pre-processing.

Table 1. Atmospheric and land surface parameters sources and preprocessing.

Parameters	Source	Spatial Resolution	Temporal Resolution	Data Preprocessing
Atmospheric Parameters				
Precipitation (Rainfall)	AMeDAS observation	Point observation	1 h	Spatial interpolation
	MLIT observation		1 h	Spatial interpolation
	Remote sensing (MTSAT based estimation)	Point observation 5 km downscaled into 1-km	1 h	Spatial interpolation and statistical downscaling
Wind	AMeDAS observation	Point observation	1 h	Spatial interpolation
Atmospheric Temperature	AMeDAS observation	Point observation	1 h	Spatial interpolation
Atmospheric Pressure	AMeDAS observation	Point observation	1 h	Spatial interpolation
Atmospheric Relative Humidity	AMeDAS observation	Point observation	1 h	Spatial interpolation
Cloud cover	JMA Mesoscale Model	25 km	3 h	Spatial Resampling
Shortwave downward radiation	Remote sensing (CERES)	20 km	~12 h	Spatial Resampling
Longwave downward radiation	Remote sensing (CERES)	20 km	~12 h	Spatial Resampling
Land surface parameters				
Land use	Remote Sensing (MODIS)	1 km	yearly	Georeferencing and spatial resampling
Surface slope	Remote Sensing (SRTM-DEM)	90 m	-	Spatial aggregation and DEM processing
Standard deviation of surface topography	Remote Sensing (SRTM-DEM)	90 m	-	Spatial aggregation and DEM processing
Flow direction	Remote Sensing (SRTM-DEM)	90 m	-	Spatial aggregation and DEM processing
Flow accumulation	Remote Sensing (SRTM-DEM)	90 m	-	Spatial aggregation and DEM processing
Surface Albedo	Remote Sensing (MODIS)	1 km	16 days	Georeferencing
Leaf Area Index	Remote Sensing (MODIS)	1 km	8 days	Georeferencing
Soil texture	FAO digital soil map of the world	Vector based at 1:5,000,000 scale	-	Georeferencing and spatial resampling

Preprints (www.preprints.org) | NOT PEER-REVIEWED | Posted: 27 September 2019 doi:10.20944/preprints201909.0312.v1

Peer-reviewed version available at Hydrology 2020, 7, 9; doi:10.3390/hydrology7010009

3. Study Area

We estimated river flow in the Ishikari River basin, which is located on Hokkaido Island, Japan. However, we only compared flash flooding in four gauged catchments situated in the Ishikari River basin: Shirai, Bebetsugawa, Beiegawa, and Upper Ishikari (see Figure 1). Data for the year 2010 were used for the MATSIRO data-forcing preparation process.

4. Methods

MODIS data were used to acquire land surface parameters in MATSIRO. Several MODIS-based data products are relevant as MATSIRO data input: leaf area index (MCD15A3), surface albedo (MCD43B3), and land cover type (MCD12Q1). Because these data are mainly delivered in Hierarchical Data Format (HDF), which is not compatible with the MATSIRO, they were converted into plain binary format.

MATSIRO uses some topographical parameters, such as the surface slope and the standard deviation of altitude in a grid cell. These parameters can be extracted from a DEM analysis of SRTM-DEM data. Suppose the surface function of DEM is defined as z = f(x,y), where x and y are the grid location of the elevation z. The first derivative in the x and y directions is respectively defined as fx = df/dx and fy = df/dy. The slope angle is calculated as:

$$\beta_s = Arc\tan\left(\sqrt{f_x^{\,2} + f_y^{\,2}}\right) \quad (1)$$

The standard deviation of subgrid topography in the grid box can be calculated using a standard deviation function during the aggregation process from the grid size of 90 m × 90 m to 1 km × 1 km. Another contribution of SRTM-DEM information into MATSIRO is related to runoff routing processes; this is made possible by implementing the TRIP, i.e., to generate the river flow direction and river flow accumulation.

Rainfall forcing data for June–September 2010 were estimated from MTSAT data. A statistical model using the MTSAT 10.8 μm channel data was implemented to estimate rainfall. A cloud type classification based on the MTSAT split window was implemented to detect Cumulonimbus (Cb) cloud [13]. The atmospheric environmental conditions, i.e., atmospheric vertical instability and the availability of precipitable water vapor that sustains Cb cloud development, were taken into account during the rainfall estimation process. Particularly for the convective rain, the statistical model was combined with the precipitable water and atmospheric vertical instability [7]. Because the estimated rainfall output preserved the native resolution of the MTSAT image (a grid of approximately 5 km), a statistical downscaling method was conducted to convert the data into a grid size of 1 km: the estimated rainfall from the MTSAT satellite was downscaled with the observed rainfall (hereafter, MTSAT downscaled).

The downscaling process combines the advantages of those two rainfall data capture systems. Rain gauge observations are the only direct source of rainfall data. However, these data are limited due to lack of distribution, particularly in remote areas. Satellite observations are indirect by nature, but they provide very good spatial coverage. By merging the benefits of these systems, the combined result is expected to be improved in accuracy, coverage, and resolution [14]. Discrepancy between the satellite-based rainfall estimation and direct observations from rain gauges can be reduced during the downscaling process through bias correction, which is based on (i) additive and (ii) multiplicative methods that are applied hourly to each station. The additive bias correction (rr^+) and multiplicative bias correction (rr^*) are respectively defined as [14]:

$$rr^+ = rr_{sat} + \overline{(rr_{obs}^i - rr_{sat}^i)} \quad (2)$$

Preprints (www.preprints.org) | NOT PEER-REVIEWED | Posted: 27 September 2019 doi:10.20944/preprints201909.0312.v1

Peer-reviewed version available at Hydrology 2020, 7, 9; doi:10.3390/hydrology7010009

$$rr^{*} = rr_{sat} \times \overline{\left(\frac{rr_{obs}^{i}}{rr_{sat}^{i}} \right)} \quad (3)$$

The first term in both equations is the satellite-based rainfall estimation. The second terms in Equations (2) and (3) represent respectively the mean bias (represented by the bar) and both the additive and multiplicative biases between the observed and estimated rainfall for each station (denoted by superscript i). The procedure for performing statistical downscaling is as follows. The observed rainfall is interpolated using the inverse distance weight method on a 1-km grid size, with a limiting distance of approximately 10 km. The satellite-based rainfall is disaggregated from a grid resolution of 5 km to 1 km. Next, the difference between additive or multiplicative is calculated: the means of both the additive and multiplicative biases for each station can be calculated by applying a 3 × 3 summation filter, divided by the number of grid points containing the bias value. The downscaled bias-corrected rainfall can be calculated using Equations (2) and (3) for the additive and multiplicative values accordingly. Here, we selected one particular bias correction method for each point grid based on the minimum difference between the bias-corrected rainfall and the observed rainfall. For grid points outside the limiting distance of the interpolation, the original estimated rainfall was assigned.

Three simulations were performed to estimate the river flow using MATSIRO; these are summarized in Table 2. A simulation using rainfall forcing data from the AMeDAS observation was conducted for 1 January–31 December 2010. This simulation generated a so-called 'restart file', which is the initial condition of the land surface hydrological condition for each time-step. The other simulations (MLIT and MTSAT downscaled rainfall) were conducted using the current restart file, but only during the period of boreal summer (1 June–30 September 2010). It is because the flash flood events mainly occurred during this period of summer. The estimated river flow was extracted from the river flow distribution at the outlet of the catchment and was finally compared with the observed discharge for August 2010.

Table 2. Summary of river flow simulations using MATSIRO.

Simulation Name	Time Duration	Rainfall Data Forcing
Simulation I	1 January–31 December 2010	AMeDAS rainfall observation
Simulation II	1 January–30 September 2010	MLIT rainfall observation
Simulation III	1 January–30 September 2010	MTSAT downscalled

5. Results and Discussion

First, the performance of the downscaled MTSAT and AMeDAS rainfall was demonstrated by comparison with the MLIT rainfall. We selected MLIT rainfall as the benchmark because this includes a denser rainfall network than AMeDAS, particularly in mountainous regions. Figure 2 presents the distribution of the AMeDAS rainfall network (white dots) and MLIT rainfall network (black dots). Because MLIT data were characterized by a denser station network over the Ishikari River basin (spacing of approximately 10 km) compared with AMeDAS (spacing of approximately 20 km), it is likely more accurate than the other rainfall measurements, and likely represents the spatial distribution of rainfall more accurately. Figure 3a,b present a scatterplot of the catchment average rainfall of MTSAT downscaled vs. MLIT rainfall, and AMeDAS rainfall vs. MLIT rainfall for the Shirai catchment. The catchment average rainfall was derived by calculating the average value of rainfall grid data which is extracted according to the catchment boundary. Similar scatter plots for the Bebetsugawa catchment are shown in Figure 3c,d, which indicate that the relationship between the MTSAT downscaled and MLIT rainfall is more accurate than the AMeDAS rainfall and the MLIT rainfall. This finding suggests that MTSAT can estimate rainfall downscaled by AMeDAS more accurately than AMeDAS alone, especially for mountainous regions.

Preprints (www.preprints.org) | NOT PEER-REVIEWED | Posted: 27 September 2019 doi:10.20944/preprints201909.0312.v1

Peer-reviewed version available at Hydrology 2020, 7, 9; doi:10.3390/hydrology7010009

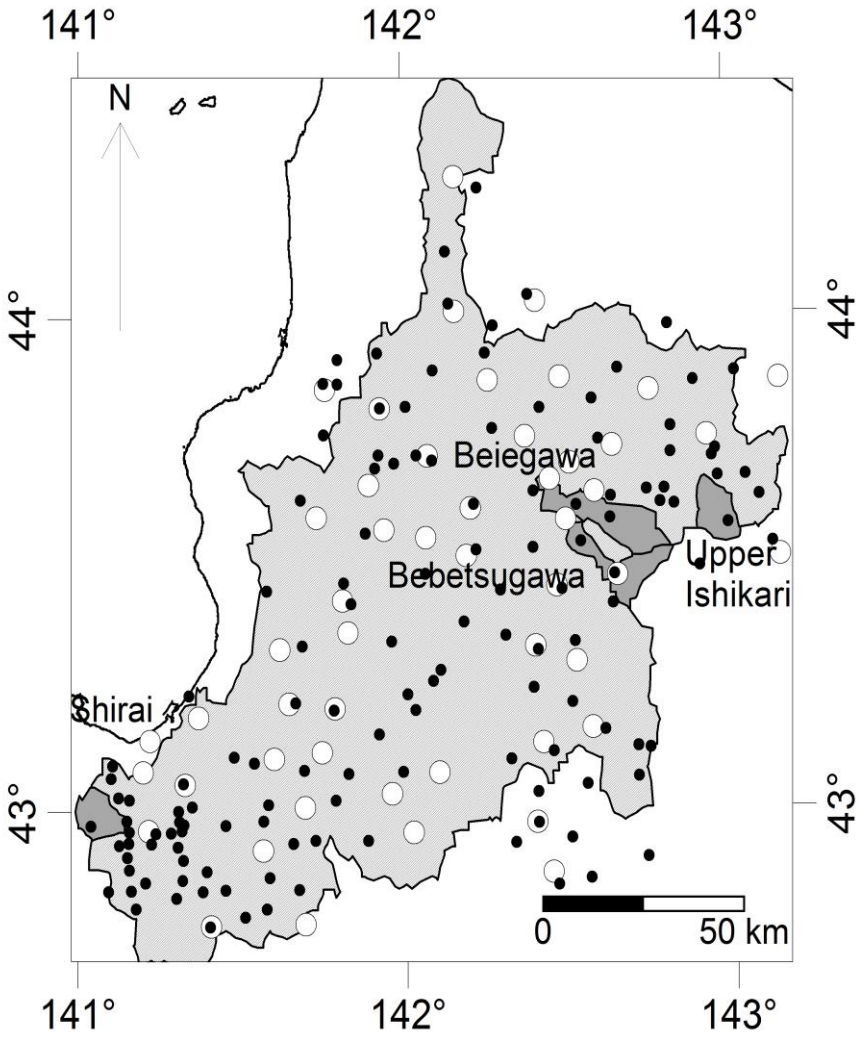

Figure 2. The locations of sub-catchments (grey shaded polygon) that are situated inside the Ishikari river basin (hatched polygon). The dots show the distribution of the AMeDAS rainfall network (white dots) and the MLIT rainfall network (black dots).

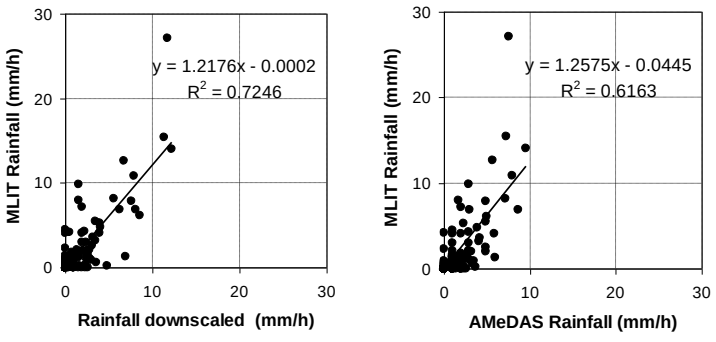

(**a**) (**b**)

Preprints (www.preprints.org) | NOT PEER-REVIEWED | Posted: 27 September 2019 doi:10.20944/preprints201909.0312.v1

Peer-reviewed version available at Hydrology 2020, 7, 9; doi:10.3390/hydrology7010009

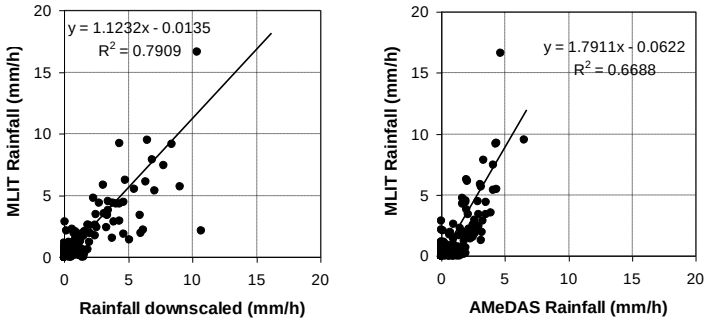

(**c**) (**d**)

Figure 3. Graphical comparison of river flow simulation results vs. observed discharge for (**a**) Shirai river and (**b**) Bebetsugawa river**.** Scatter plot of catchment average hourly rainfall: (**a**,**c**) MTSAT downscaled vs. MLIT rainfall, (**b**) AMeDAS rainfall vs. MLIT rainfall in August 2010 for (**a**,**b**) Shirai river catchment, and (**c**,**d**) Bebetsugawa river catchment.

A comparison of the hourly estimated river discharge as the result of river flow simulations using MATSIRO with the observed discharge can be presented in two ways: graphical comparison, and comparison of statistical performance by measuring correlation, bias, and root mean square (RMS) [15]. Since the objective of this study is to simulate the flash flood by using several types of rainfall forcing, for the purpose of comparison we only consider a flash flood event which was occurred during a heavy rainfall event from 23 and 24 August 2010. Figure 4a–d show the peak discharge hydrographs for the Shirai, Bebetsugawa, Upper Ishikari and Beiegawa rivers, respectively. These flood events are classified as flash floods due to the short time to peak discharge and the relatively high peak discharge. From the Figure 4, it can be examined that the time to peak of discharge is about 1 to 6 h and peak of discharge which is detected by simulation is about 1 to 2 h earlier than the observation. The graphical comparison of the river flow simulations demonstrate that estimating discharge using MLIT rainfall is the best in showing the peak discharge pattern, especially for the Shirai and Bebetsugawa rivers. This result is due to the fact that MLIT has a relatively dense rainfall network compared with AMeDAS, so it can more accurately represent the rainfall distribution. The second-best method for estimating discharge is using downscaled MTSAT, and the worst is using AMeDAS rainfall. These results are consistent with the previous finding, with regard for providing flash flood information about ungauged catchments, the use of downscaled MTSAT for rainfall forcing is more accurate than solely using AMeDAS rainfall. Since the mostly areas have faced problem in lacking rainfall networks, the downscaled MTSAT results may be useful to overcome such problem. MTSAT is able to represent the rainfall distribution well, but it is less accurate in predicting the amount of rainfall. This limitation was improved by adjusting bias based on observed rainfall, even when these are acquired with sparse station distribution.

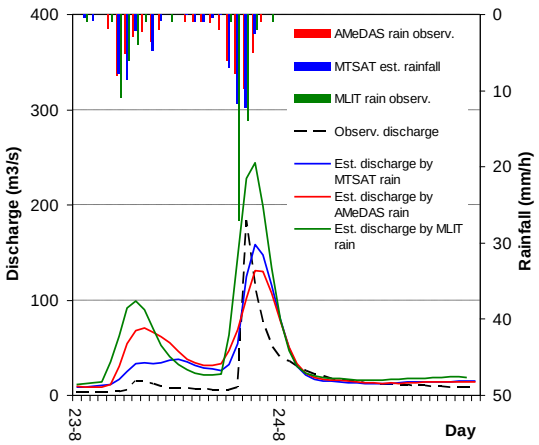

(**a**)

Preprints (www.preprints.org) | NOT PEER-REVIEWED | Posted: 27 September 2019 doi:10.20944/preprints201909.0312.v1

Peer-reviewed version available at Hydrology 2020, 7, 9; doi:10.3390/hydrology7010009

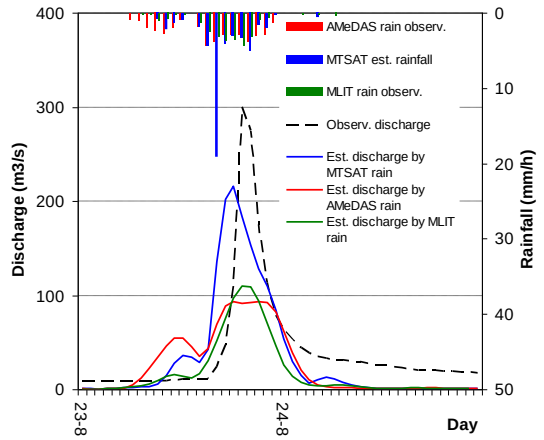

(**b**)

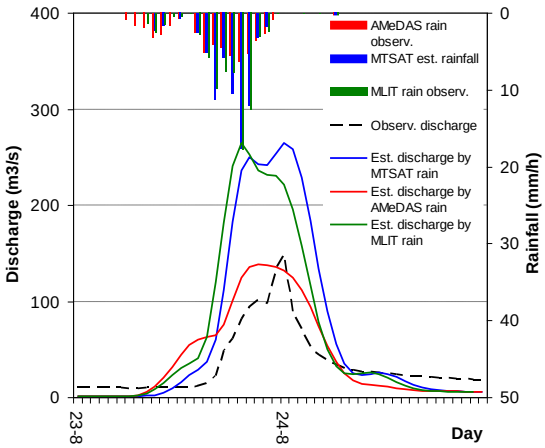

(**c**)

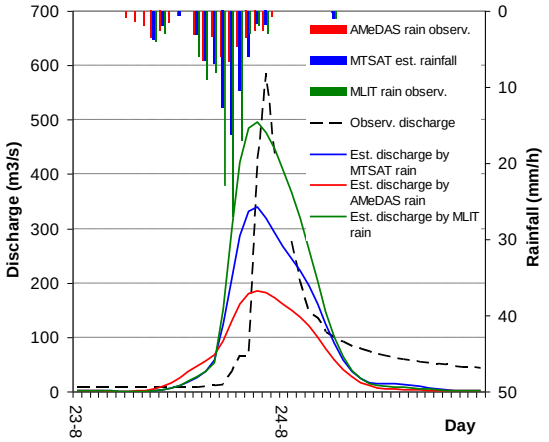

(**d**)

Figure 4. Peak discharge during a heavy rainfall event on 23–24 August 2010 at the catchment outlets of (**a**) Shirai; (**b**) Upper Ishikari; (**c**) Beiegawa and (**d**) Bebetsugawa river.

The graphical comparison was confirmed by a statistical performance calculation, as presented in Table 3. This statistics are calculated only for the period of flash flood event i.e., 23 and 24 August 2010. Numbers that have been bolded indicate the most accurate statistics. The results suggest that discharge simulated using downscaled MTSAT is reasonably comparable with MLIT rainfall-based simulated discharge, and that both of these methods are much better than using AMeDAS rainfall alone as input forcing.

Preprints (www.preprints.org) | NOT PEER-REVIEWED | Posted: 27 September 2019 doi:10.20944/preprints201909.0312.v1

Peer-reviewed version available at Hydrology 2020, 7, 9; doi:10.3390/hydrology7010009

Table 3. Comparison of the performance of simulated vs. observed river discharge.

Catchment's Name	Simulation I			Simulation II			Simulation III		
	Cor	Bias (m^3/s)	RMS (m^3/s)	Cor	Bias (m^3/s)	RMS (m^3/s)	Cor	Bias (m^3/s)	RMS (m^3/s)
Shirai	0.68	15.9	29.7	**0.95**	27.6	48.0	0.82	**12.2**	**23.3**
Upper Ishikari	0.89	−15.8	48.0	**0.90**	−23.0	**43.0**	0.73	**−8.2**	44.0
Beiegawa	0.96	**6.9**	**24.4**	**0.97**	29.0	62.9	0.94	31.5	68.1
Bebetsugawa	**0.99**	−30.1	94.8	0.98	29.4	117.6	0.75	**−3.2**	**88.6**

6. Conclusions

A river flow simulation was conducted using the MATSIRO land surface model in the Ishikari River basin. Input forcing data were a combination of direct observations from the AMeDAS network and data derived from remote sensing. A statistical downscaling procedure was applied to MTSAT satellite-based rainfall estimation by merging these data with the interpolated AMeDAS rainfall. We compared the MTSAT downscaled and AMeDAS interpolated rainfall with the MLIT rainfall, which we assumed would represent the rainfall distribution more accurately than AMeDAS due itsthe denser station distribution. The comparison revealed that downscaled MTSAT is reasonably comparable with MLIT rainfall and is better than using AMeDAS data alone. The river flow simulations for the four catchment areas in the Ishikari basin demonstrate that using MLIT rainfall to estimate peak discharge provides more accurate results than the other methods. However, the downscaled MTSAT is better as input forcing in a physically based model, because its accuracy is roughly comparable with relatively dense rain gauge networks such as the MLIT. Moreover, many regions have sparse rain gauges, and this challenge can be overcome by merging these data with MTSAT rainfall estimation.

Author Contributions:

Funding: This study was partially supported by the Research Program on Climate Change Adaptation, Ministry of Education, Culture, Sports, Science and Technology, Japan (SI-CAT/MEXT).

Conflicts of Interest:

The authors declare no conflict of interest.

References

1. Yousef, A.M.; Pradhan, B.; Hassan, A.M. Flash flood risk estimation along the St. Katherine road, southern Sinai, Egypt using GIS based morphometry and satellite imagery. *Environ. Earth Sci.* **2011**, *62*, 611–623, doi:10.1007/s12665-010-0551-1, 2010.
2. Alfieri, L.; Thielen, J.; Pappenbeger, F. Ensemble hydro-meteorological simulation for flash flood early detection in Southern Switzerland. *J. Hydrol*. **2012**, *424*, 143–153, doi:10.1016/j.hydrol.2011.12.038.
3. Baskar, N.R.; French, M.N.; Kiyamah, G.K. Characterization of flash flood in Eastern Kentucky. *J. Hydrol. Eng*. **2000**, *5*, 327–331.
4. Kim, E.S.; Choi, H.I. Estimation of the relative severity of floods in small ungauged catchments for preliminary observation on Flash flood preparedness: A case study in Korea. *Int. J. Environ. Res. Public Health* **2012**, *9*, 1507–1522.
5. Haile, A.T.; Rientjes, T.; Gieske, A.; Gebremichael, M. Multispectral remote sensing for rainfall detection and estimation at the source of the Blue Nile river. *Int. J. Appl. Earth Obs. Geoinf*. **2010**, *12*, S76–S82.
6. Kinoti, J.; Su, Z.; Woldai, T.; Maathuis, B. Estimation of spatial-temporal rainfall distribution using remote sensing techniques: A case study of Makanya catchment, Tanzania. *Int. J. Appl. Earth Obs. Geoinf.* **2010**, *12*, S90–S99.
7. Suseno, D.P.Y.; Yamada, T.J. The role of GPS precipitable water vapor and atmospheric vertical stability index in the statistically-based rainfall estimation using MTSAT data. *J. Hydrometerol.* **2013**, *14*, 1922–1932.
8. Wardah, T.; Abu Bakar, S.H.; Bardosy, A.; Maznorian, M. Use of geostationary meteorological satellite images in convective rain estimation for flash-flood forecasting. *J. Hydrol*. **2008**, *356*, 283–298.
9. Takata, K.; Emori, S.; Watanabe, T. Development of the minimal advance treatments of surface interaction and runoff. *Glob. Planet. Chang.* **2003**, *38*, 209–222.

Preprints (www.preprints.org) | NOT PEER-REVIEWED | Posted: 27 September 2019 doi:10.20944/preprints201909.0312.v1

Peer-reviewed version available at Hydrology 2020, 7, 9; doi:10.3390/hydrology7010009

10. Pokhrel, Y.; Hanasaki, N.; Koirala, S.; Cho, J.; Yeh, P.; Kim, H.; Oki, T. Incorporating Anthropogenic Water Regulation Modules into a Land Surface Model. *J. Hydrometeor*. **2012**, *13*, 255–269.
11. Koirala, S.; Yamada, H.; Yeh, P.; Oki, T.; Hirabayashi, Y.; Kanae, S. Global Simulation Of Groundwater Recharge, Water Table Depth, And Low Flow Using A Land Surface Model With Groundwater Representation. *Annu. J. Hydraul. Eng.* **2012**, *56*, doi:10.2208/jscejhe.68.I_211.
12. Oki, T.Y.; Sud, C. Design of Total Runoff Integrating Pathways (TRIP)-A global river channel network. *Earth Interact.* **1998**, *2*, 1–36.
13. Suseno, D.P.Y.; Yamada, T.J. Two-dimensional, threshold-based cloud type classification using MTSAT data. *Remote Sens. Lett.* **2012**, *3*, 737–746.
14. Vila, D.A.; Goncalves, L.G.; Toll, D.L.; Rozante, J.B. Statistical Evaluation of Combined Daily Gauge Observation and Rainfall Satellite Estimates over Continental South America. *J. Hydrometeorol.* **2009**, *10*, 533–543.
15. Ebert, E.E. 2007. Forecast Verification—Issues, Methods and FAQ. Available online: http://www.cawcr.gov.au/projects/verification/ (accessed on 20 September 2019).